Electronic Supplementary Material (ESI) for Dalton Transactions.

Supporting Information

Pursuing unprecedent anisotropic morphologies of halide-free Pd nanoparticles by tuning nucleation and growth

Federico Spolaore,[a,b] Francesca Tajoli,[a] Maria Chiara Dalconi,[c] Christoph Hengst,[b] Franz Dornhaus[b] and Silvia Gross*[a,d,e]

Table of content:

[a] *Department of Chemical Sciences, University of Padova, Via Marzolo 1, 35131, Padova, Italy*
[b] *Department Automotive Catalysts, Umicore AG & Co. KG, Rdenbacher Chaussee 4, 63457, Hanau, Germany*
[c] *Department of Geosciences, University of Padova, Via G. Gradenigo 6, 35131, Padova, Italy*
[d] *Interdepartmental Centre Giorgio Levi Cases for Energy Economics and Technology, University of Padova, Via Marzolo 9, 35131, Padova, Italy*
[e] *Karlsruher Institut für Technologie (KIT), Institut für Technische Chemie und Polymerchemie (ITCP), Engesserstr. 20, 76131 Karlsruhe, Germany*

Table S1**:** Size features of Sample A, B and C obtained by TEM after 0.5 h, 1 h and 2 h reaction time. Feret diameter and cylindrical length are given for well-defined structures and worm-like nanostructures, respectively, calculated as described in Figure S2. The standard deviations σ are also reported.

Sample	Reaction time [h]	Feret diameter [nm]	σ [nm]	Calculated cylindrical length [nm]	σ [nm]
A	0.5	-	-	16	13
	1	-	-	17	13
	2	-	-	18	14
B	0.5	11.5	3.3	18	12
	1	10.9	2.9	24	16
	2	11.1	2.7	22	14
C	0.5	7.3	2.8	-	-
	1	8.1	2.9	-	-
	2	8.6	2.9	-	-

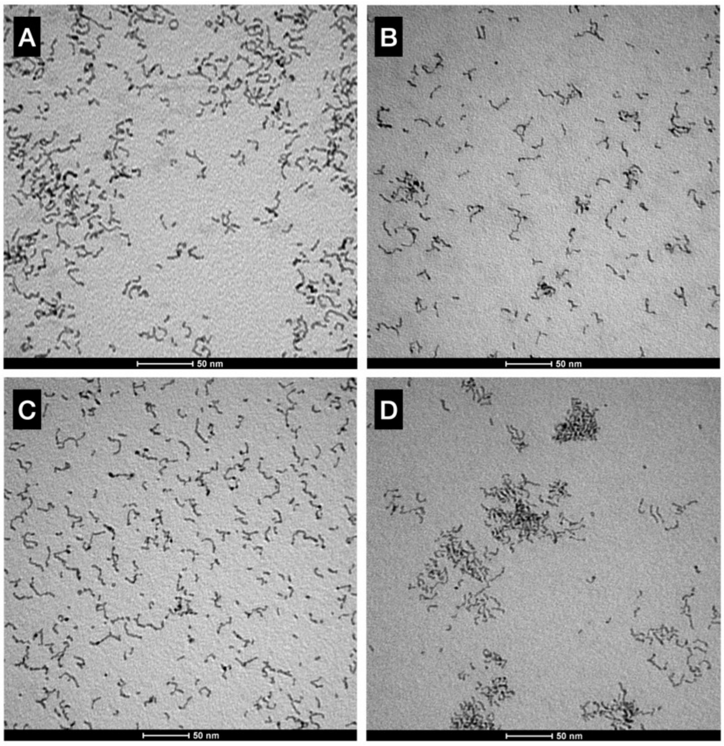

Figure S1: TEM analysis of four different samples at apparent basic pH values with different Pd/$Ca(NO_3)_2$ molar ratio, namely 1/0 (A), 1/3 (B), 1/6 (C) and 1/9 (D). Independently from the NO_3^- or Ca^{2+} content, worm-like nanostructures were obtained carrying out the reaction at basic pH values.

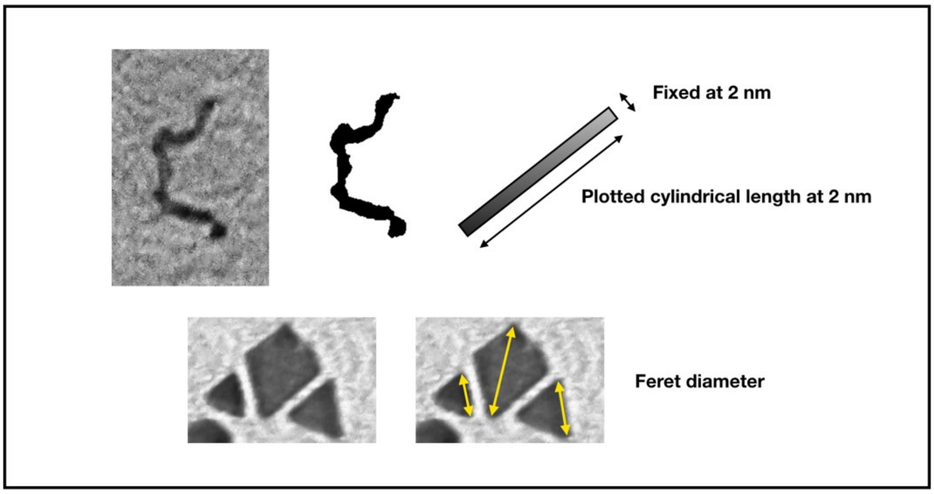

Figure S2: Sketch of the method used to calculate the *cylindrical length* for the worm-like nanostructures, starting from the area of the NPs, measured after a proper image segmentation. Thickness was fixed to 2 nm since it was the measured average thickness. Below, a sketch of the *maximum Feret diameter* used to calculate the average particle size for the geometrically defined nanostructures. The Feret diameter is expressed as the maximum distance between two tangent lines on opposite side of particle profiles to the surface of the NPs.

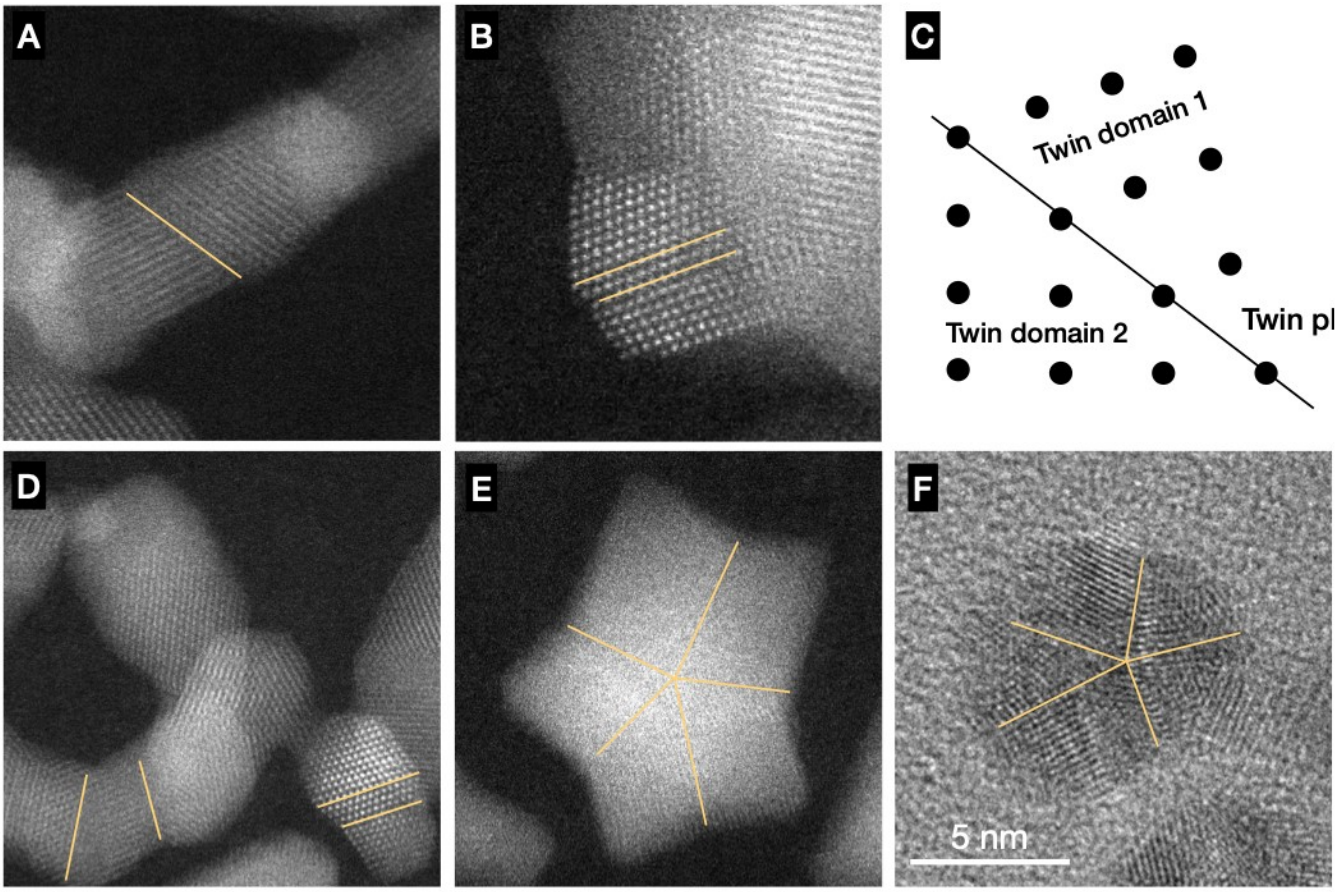

Figure S3: STEM of Sample A (figure A). STEM of Sample B (figure B and D). Sketch of a twin plane with the different twin domains (image C). STEM and HRTEM of Sample C (figure E and F) highlighting the presence of 5-fold twins.

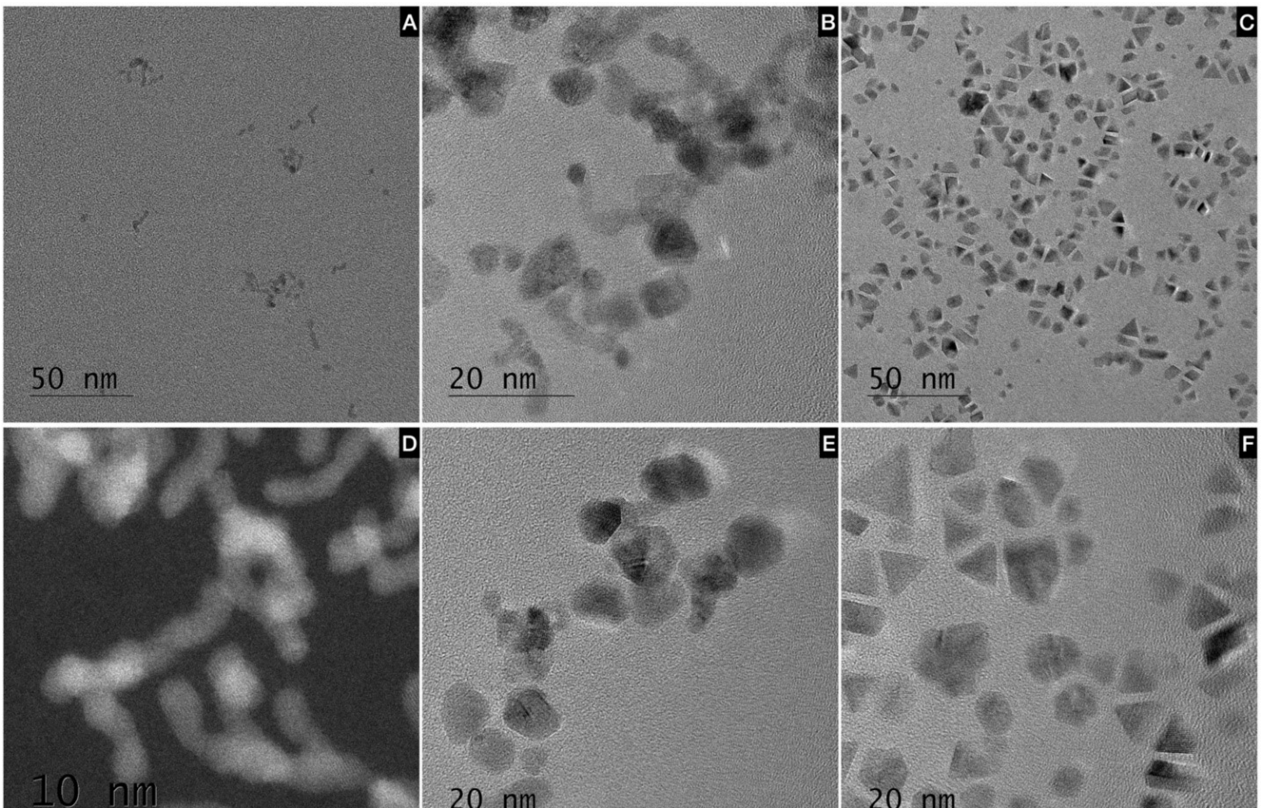

Figure S4: HRTEM and STEM of Sample A (figures A,D), B (figures B,E) and C (figures C,F).

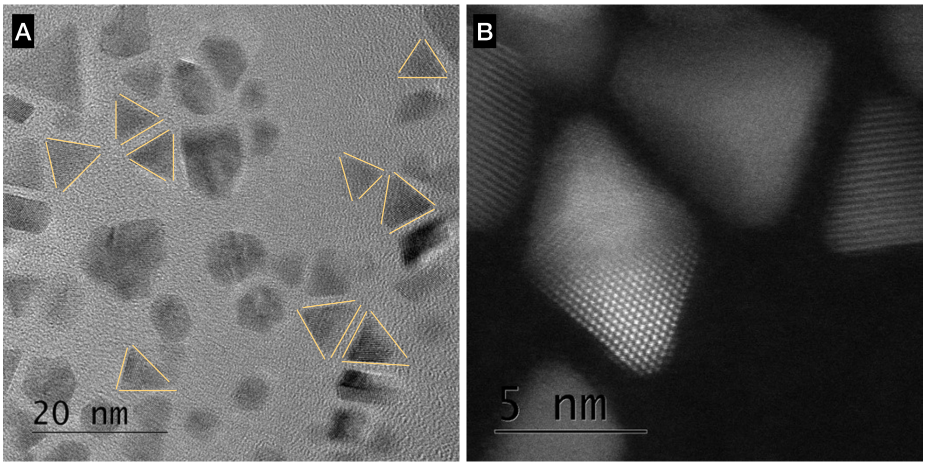

Figure S5: HRTEM and STEM of Sample C, highlighting the presence of tetrahedra and octahedra in the sample.

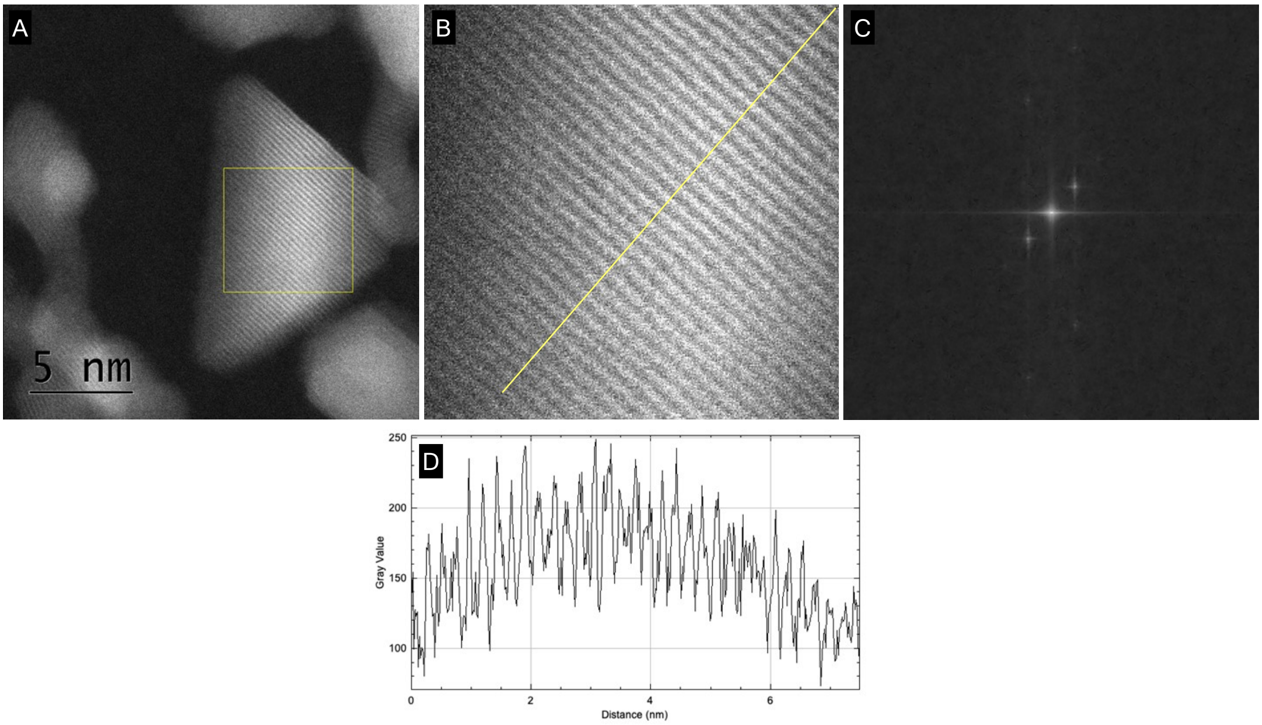

Figure S6: STEM of a portion of Sample B (figure A); Enlargement of the atomic packing characteristic of a plane in a <111> orientation (figure B); FFT of the magnified portion (figure C) and interplanar distances measured, along a 7.5 nm line (yellow line in B) perpendicular to 33 planes resulting in an interplanar distance of 0.23 nm, characteristic of planes in a <111> orientation (figure D).

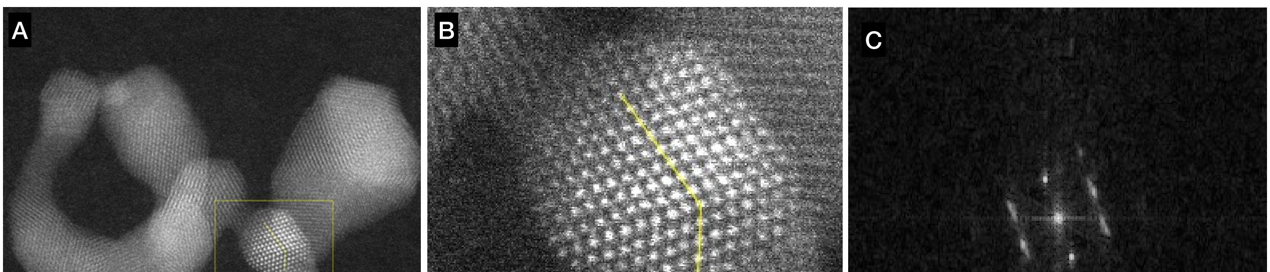

Figure S7: STEM of a portion of Sample B (figure A); Enlargement of the atomic packing with twinned planes oriented towards different directions (figure B); FFT of the magnified portion (figure C); Interplanar distances measured, along two lines (yellow lines in B) perpendicular to 4 and 8 planes respectively, resulting in lattice distances of 0.27 nm and 0.25 nm, characteristic of high Miller indices planes, likely the (110) and (311) ones (figures D and E).

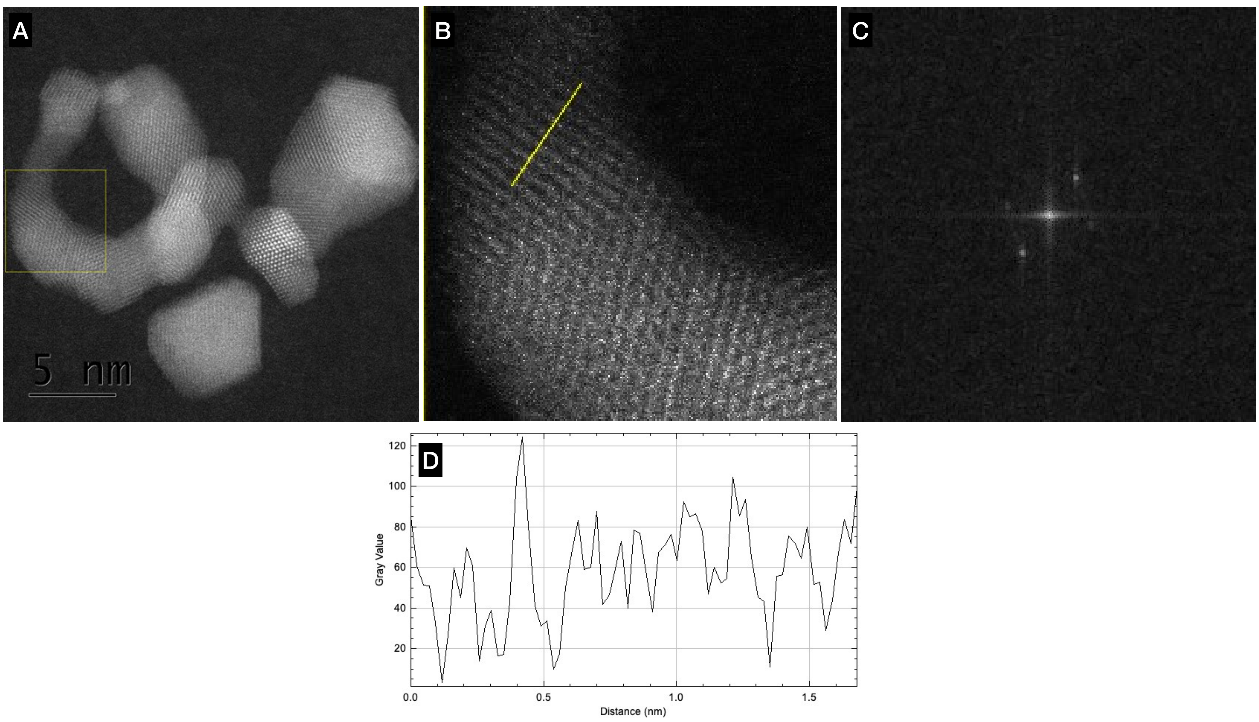

Figure S8: STEM of a portion of Sample B (figure A); Enlargement of the atomic packing characteristic of a plane in a <100> orientation (figure B); FFT of the magnified portion (figure C) and interplanar distances measured, along a 1.68 nm line (yellow line in B) perpendicular to 8 planes resulting in an interplanar distance of 0.20 nm, characteristic of planes in a <200> orientation (figure D).

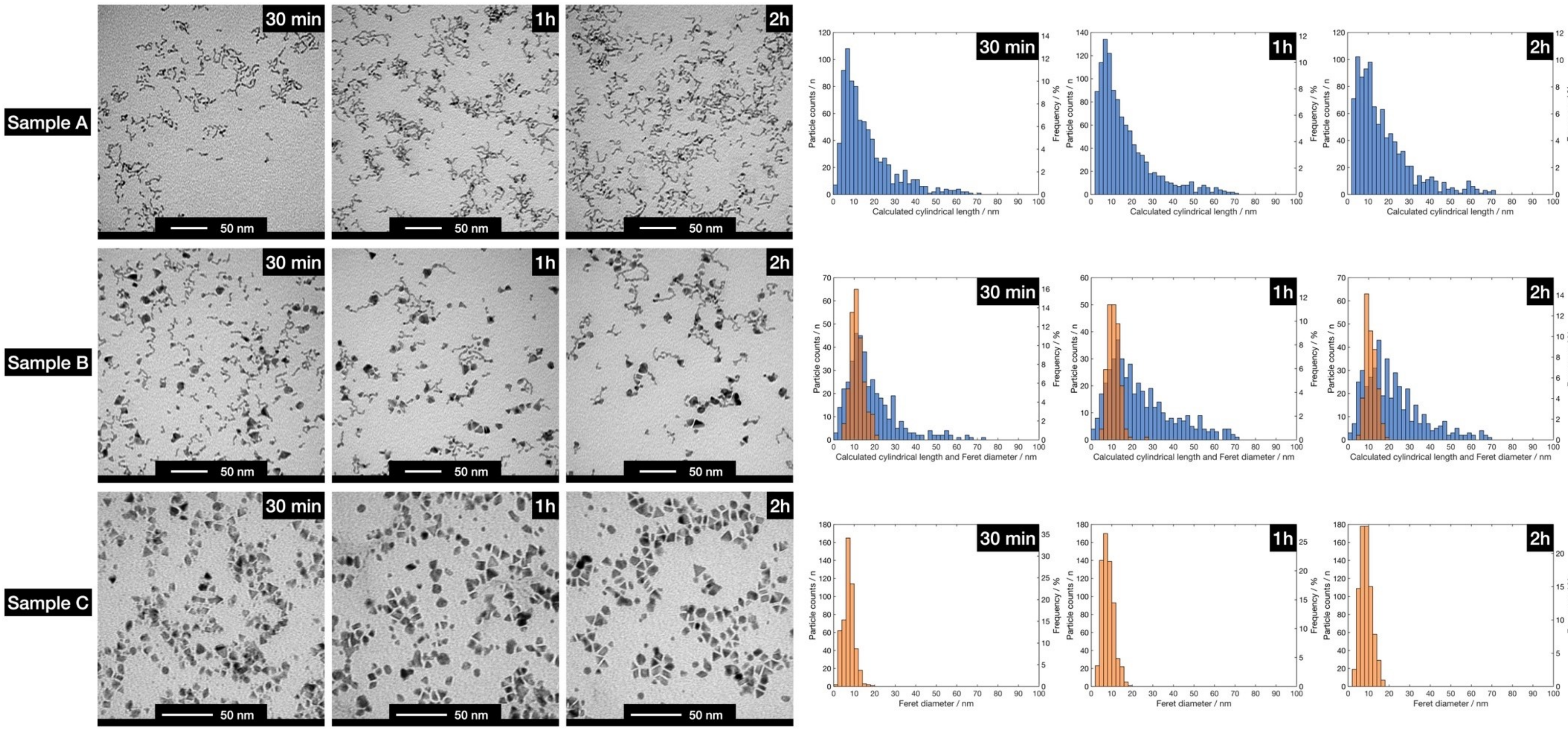

Figure S9: TEM images and particle size distributions of Samples A, B and C. Samples were sampled after 30 min, 1 h and 2 h from the initial colour change. Two distinct length descriptors were used. The Feret diameter (orange) was better suited for more geometrically defined structures, while the calculated cylindrical length (blue) from the analysed area was used for worm-like nanostructures. Particle size distributions were calculated based on at least 500 counts. Scale bars are 50 nm for all reported TEM images.

Deposition over γ-alumina, TG-MS and DRIFT study

The adsorption of the catalytically active component on porous supports is an important step in the preparation of supported catalysts. The deposition is ruled by (i) the pH of the impregnating suspension, on (ii) the point of zero charge (PZC) of the support surface, and on (iii) the nature of the metal particles.[1,2] By changing the pH of the slurry containing both components, the nanostructures' adsorption is accordingly modified. The effect of the pH on the metal adsorption is driven by the surface charge of the support, such as in the case of the γ-alumina used in this study.[1] Indeed, the hydroxyl groups at the surface of the support behave as Brønsted acids or bases undergoing surface ionization reactions.[1]

By switching the pH of γ-alumina (isoelectric point around pH = 9[3]) slurry to about 6 with addition of diluted HNO_3 (6.5 wt%), the nanostructures were deposited over the support with a final metal loading of 1 wt.% (verified by ICP-OES), taking advantage of the electrostatic interaction between the negatively charged Pd NPs and the positively charged alumina particles at these pH values. The suspensions were then dried at 105 °C/12 h, obtaining fine powders. A portion of Sample B, comprising both nanostructures deposited on alumina, was analysed by Thermal Gravimetric Mass Spectrometry (TG-MS) analysis coupled with Differential Scanning Calorimetry (DSC) to reveal the decomposition traces of the leftover EG. A heating step test (50-250 °C, 10 K/min, 50 K/step, 30 min holding time per step, final temperature 600 °C) was performed in order to study the persistence of the EG in the system and to reveal the minimum required temperature necessary to decompose all the traces of organics. As evidenced in Figure S10, sharp exothermic decompositions were repeatedly observed starting at around 150 °C up to 250 °C (end of the step test). Whereas the boiling point of EG is around 200 °C at 101.3 kPa, the presence of ethylene glycol was still revealed at temperatures as high or above as 250 °C, culminating with a final exothermic event at around 300 °C.

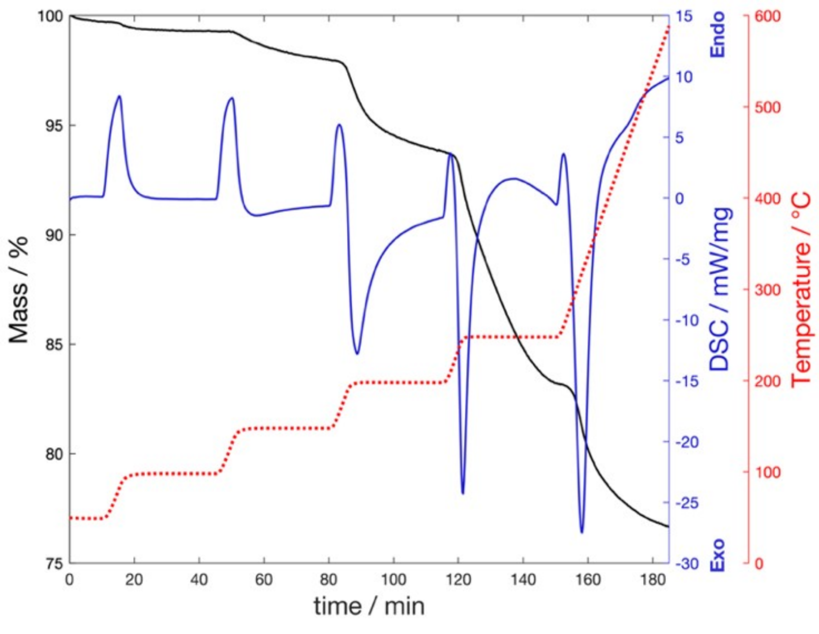

Figure S10: TG-MS coupled with DSC study of a selected sample of Pd NPs (Sample B) deposited on γ-alumina. Temperature (red), calorimetry measurements (blue) and mass loss (black) during a step test starting at 50 °C up to 250 °C followed by a ramp to 600 °C performed to follow the decomposition of EG.

The infrared spectrum of adsorbed CO on Pd NPs is a long-debated topic in literature.[4,5,6] It is generally agreed that the resulting signals position and intensity of adsorbed CO are modified by many contributions, such as by the type of metal, by the degree of coordinative unsaturation of the adsorption sites, by the presence of co-adsorbates and by the degree of CO surface coverage.[5] Linearly adsorbing CO on flat surfaces requires the lowest enthalpy of adsorption compared to bridged sites, characterised also by a narrow linewidth and symmetric line shape at around 2077 cm^{-1}, indicative of a well-defined adsorption geometry.[6] A closer inspection on the measured spectra reveal only weak, if not total absence, of any feature at around 2050-2100 cm^{-1} (highlighted in green in Figure S11) therefore pointing out the absence of large Pd nanocrystals in all three samples.[7] Indeed, it was reported that on-top CO cannot be populated at low partial pressures of CO on small Pd crystallites.[6] In addition to the signals assigned to linearly adsorbed CO molecules, different contributions were previously observed: (i) a broad band at around 1838 cm^{-1}, ascribed to μ_3 hollow-bonded CO in threefold sites (purple highlighting in Figure S11), (ii) one at 1896 cm−1 (also observed as a broadband 1923 cm^{-1} in another study) ascribed to μ_3 hollow-bonded CO on Pd(111) or to a μ_2 bridge-bonded CO on Pd(100) facets (orange highlighting in Figure S11), (iii) a sharp band observed at 1969-1984 cm^{-1}, assigned to bridge-bonded CO on Pd(100) facets or to CO bonded with a bridging fashion to edges and steps (blue highlighting in Figure S11).[4,5,6]

The recorded spectra slightly differ from those typically reported for CO adsorbed on Pd/γ-Al_2O_3 catalysts, and the differences are likely to be ascribed to the finite dimensions of the prepared Pd NPs.[4,5] The spectra of Figure S11 instead shows prominent νCO bands in the 1800-2000 cm^{-1} region, previously ascribed in literature to bridging CO species.[4,5] In the three reported spectra there is no apparent linear trend with the varying crystal shapes. Both the peculiar shapes, enclosing different facets as well as corner and edges, the possible presence of EG residues and the overlapping site and adsorption-moieties dependent bands that CO possesses, made difficult the assignments of the overlapping bands. Further studies are therefore required to

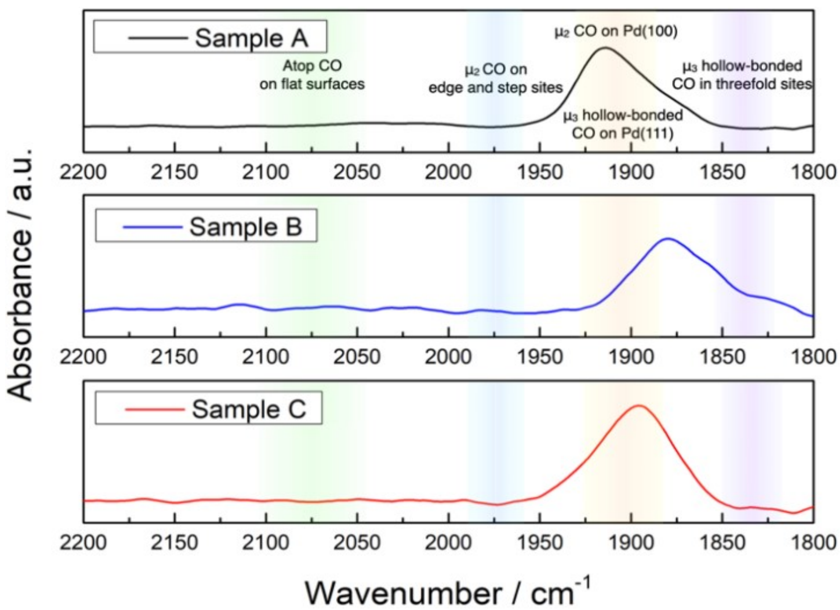

Figure S11: DRIFT spectroscopy for Samples A (black), B (blue) and C (red), with superimposed the regions attributed to the various contribution of νCO as reported in [4] and [6].

discriminate the varying ratio of the intensities for the μ_3 hollow-bonded CO and μ_3 bridge-bonded CO on (111) planes. Nevertheless, despite the overlap of vibrational frequencies for bridged CO molecules on different adsorption sites, there is a considerable contrast between the overall chemisorbed CO spectra for the supported Pd nanocrystals against other literature samples where big Pd NPs were analysed, which demonstrates how DRIFT measurements can be an additional sensitive tool to assess the changes in metal particle size and shape, which reflects on a different ratio of adsorption sites.

References

1 J. Regalbuto, *Catalyst Preparation*, CRC Press, Boca Raton, 2007.

2 G. Marzun, C. Streich, S. Jendrzej, S. Barcikowski and P. Wagener, *Langmuir*, 2014, **30**, 11928–11936.

3 G. A. Parks, *Chem. Rev.*, 1965, **65**, 177–198.

4 M. J. Kelly, J. Kim, G. W. Roberts and H. H. Lamb, *Top. Catal.*, 2008, **49**, 178–186.

5 N. Sheppard and C. De La Cruz, *Catal. Today*, 2001, **70**, 3–13.

6 T. Lear, R. Marshall, J. Antonio Lopez-Sanchez, S. D. Jackson, T. M. Klapötke, M. Bäumer, G. Rupprechter, H.-J. Freund and D. Lennon, *J. Chem. Phys.*, 2005, **123**, 174706.

7 A. M. Bradshaw and F. M. Hoffmann, *Surf. Sci.*, 1978, **72**, 513–535.